Probing Metastable Space-Charge Potentials in a Wide Band Gap Semiconductor

Artur Lozovoi [1,*] Harishankar Jayakumar,[1,*] Damon Daw [1,2] Ayesha Lakra [1] and Carlos A. Meriles [1,2,†]

[1]*Department of Physics, CUNY-City College of New York, New York, New York 10031, USA*
[2]*CUNY-Graduate Center, New York, New York 10016, USA*

While the study of space-charge potentials has a long history, present models are largely based on the notion of steady state equilibrium, ill-suited to describe wide band gap semiconductors with moderate to low concentrations of defects. Here we build on color centers in diamond both to locally inject carriers into the crystal and probe their evolution as they propagate in the presence of external and internal potentials. We witness the formation of metastable charge patterns whose shape—and concomitant field—can be engineered through the timing of carrier injection and applied voltages. With the help of previously crafted charge patterns, we unveil a rich interplay between local and extended sources of space-charge field, which we then exploit to show space-charge-induced carrier guiding.

Charge transport in semiconductor devices—including solar cells, light emitting diodes, and other energy-conversion systems—emerges from a subtle interplay between injected carriers and the type and concentration of dopants and traps present in the sample. Given the intimate connection between electric field and carrier propagation, the formation of space-charge potentials is central to gaining a full understanding of transport, even in the limit of defect-free materials as early recognized by Mott and Gurney [1]. More broadly, dopant ionization and charge trapping combine to yield complex space-charge distributions within the semiconductor, which, in turn, define the current response I to an externally applied voltage V. Describing this response—especially for low and intermediate voltages where systems depart from the Mott-Gurney model—has been the subject of work spanning many decades [2–4]. Nonetheless, a general model that correctly reproduces experimental observations without invoking *ad hoc* heterogeneity in the distribution of intrabandgap states has been formulated only recently [5].

Implicitly or explicitly, much of the present formalism rests on the assumption that, after a sufficiently long time, the system reaches a "steady state," where an effective Fermi level can be defined. In the same vein, the sample is conjectured to start from a thermodynamic equilibrium defining, e.g., the fraction of ionized donors or charged traps. It is precisely the change relative to these equilibrium configurations that governs the formation of space-charge potentials in the presence of externally applied fields. While this framework has undeniably proven useful, it is not uncommon, however, to find situations where defects adopt metastable charge states featuring virtually infinite lifetimes. This is often the case in wide band gap semiconductors hosting deep donors and acceptors, whose charge can be locally altered, e.g., with the help of optical

pulses [6,7]. In this regime, the notion of thermodynamic equilibrium throughout the semiconductor, with or without external fields, breaks down. Further, experimental approaches sensitive to spatial averages—the case for I-V measurements [8]—or selectively applicable to surfaces—such as scanning-probe-assisted methods [9,10]—become inadequate, and strategies capable of providing local space-charge information must instead be sought.

As a first step to implementing these ideas, here we use confocal fluorescence microscopy to visualize the dynamics of space-charge formation in diamond. Specifically, we exploit the nitrogen-vacancy (NV) color center as a local probe to reveal charge carrier dynamics in the presence of externally applied voltages. Combining local optical excitation and fluorescent imaging in areas around the point of illumination, we induce and observe the formation of spatial NV fluorescence patterns, whose shapes—themselves a function of the applied electric potentials—allow us to capture the genesis and spatial distribution of space-charge fields. From our experiments, we conclude these fields can reach values comparable to those applied externally (here exceeding 10^6 V/m). Further, we use time-resolved potentials and optical excitation to show that space-charge fields profoundly depend on the preparation protocol, an observation we subsequently build upon to confine and guide carrier propagation.

Figure 1(a) shows a schematic of our experimental setup [11]: We use a custom-made confocal fluorescence microscope combining green (520 nm) and orange (594 nm) lasers, whose timing we control with the help of on-off logic pulses; to reconstruct a fluorescence image, we scan the orange beam across the sample via a precision galvo system. We use a pair of surface metal electrodes connected to a high-voltage power supply and a homemade, high-speed switch to create variable, time-dependent electric
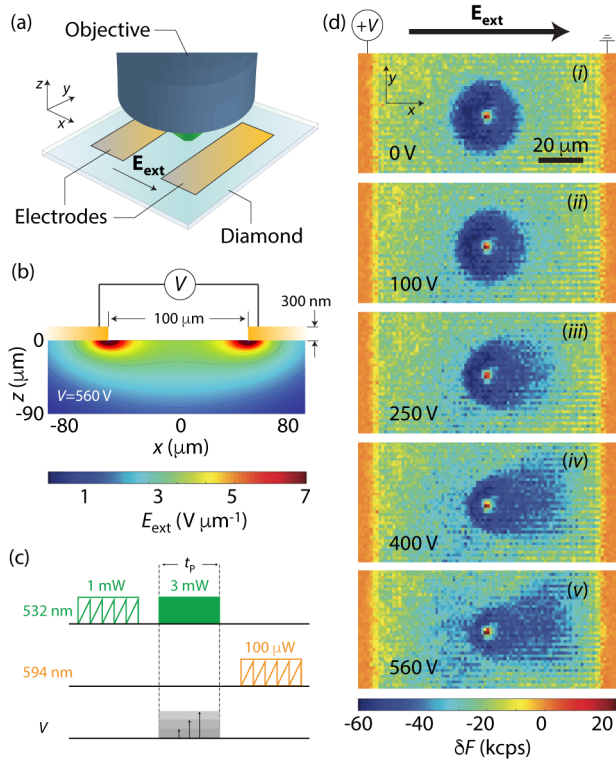
FIG. 1. Visualizing charge dynamics under constant potentials. (a) Schematics of the experimental setup. We accelerate photogenerated carriers using a pair of planar electrodes patterned on the diamond surface. (b) Calculated electric field within diamond assuming $V = 560$ V. (c) Experimental protocol; zigzags indicate laser scans and solid squares correspond to laser parks. (d) Differential NV$^-$ fluorescence δF as a function of position after a green laser park at the image midpoint for different applied voltages; the laser parking time is $t_P = 1$ min and the arrow denotes the direction of the externally applied electric field $\mathbf{E}$. The growing dark tail corresponds to the acceleration of holes toward the right, from high to low potentials.

fields in a section of the crystal [Fig. 1(b)]. All our measurements below are carried out at room temperature within the 100 μm gap separating the metal pads; we focus the laser beams 10 μm below the diamond surface, with an axial (i.e., depth) resolution of ~3 μm. Throughout the present experiments, we investigate a type 1b synthetic diamond (DDK) grown via chemical vapor deposition; the nitrogen concentration is 0.25 ppm [12], mostly in the form of neutral substitutional defects or "P1 centers."

In the absence of additional sample treatment, only a small fraction of substitutional nitrogen—about one in a hundred [13]—combine with intrinsic vacancies during crystal growth to form NV centers. Unlike P1 centers—which are optically dark—NVs have a bright fluorescence spectrum spanning the near infrared [14]. In the presence of green illumination, two-step one-photon processes interconvert NVs between their neutral and negatively charged states [15], producing in the process equal amounts of carriers of either sign, i.e., ionization of an individual

NV$^-$ leads to injection of one electron, whereas NV^0 recombination produces a free hole. Therefore, even if their concentration is comparatively low, NVs can act as optically activated charge pumps able to provide an endless stream of carriers from a predefined (though arbitrary) location in the crystal. Furthermore, because the fluorescence spectra from neutral and negatively charged NVs overlap only partially, we can make the readout of our microscope selective to only one charge state, which, as we show below, makes it possible to monitor the drift of photogenerated carriers in the applied electric field prior to recapture in a trap.

Figure 1(c) describes our measurement protocol: To charge initialize the NVs, we first scan the green laser throughout the area between the two electrodes. Because the rate of NV$^-$ photoionization is lower than the rate of NV^0 recombination, green illumination leaves the NV ensemble preferentially in the negatively charged state [15] (~75%). We subsequently park the green beam at the midpoint in the interelectrode gap and simultaneously apply a variable voltage to the metal pads. To image the ensuing NV$^-$ spatial pattern, we scan the orange laser beam across the area of interest. Although orange excitation can lead to NV$^-$ ionization, this process is inefficient at 594 nm [15], implying that a proper selection of the scan parameters (e.g., laser intensity, scanning speed) brings the impact of the readout laser on the NV ensemble to a minimum.

Figure 1(d) summarizes a series of measurements under variable voltages for a green laser park time of 60 s. Rather than the absolute photon counts, images display the differential fluorescence δF obtained upon subtraction of the equivalent fluorescence image in the absence of a green laser park. This procedure allows us to eliminate distortions introduced by uneven excitation and photon collection efficiencies throughout the large field of view required herein (spanning the full interelectrode gap).

In the absence of externally applied fields, carriers of both signs diffuse radially away from the area under illumination toward the bulk of the crystal where they can be recaptured, both by NVs and other defects. Nitrogen-vacancy centers surrounding the point of green excitation transform efficiently into neutral via trapping of diffusing holes, a process likely amplified by Coulombic attraction [16] toward NV$^-$. By contrast, NV^0 recombination via electron capture is negligible [11], thus leading to the formation of a dark, NV^0-rich "halo" concentric with the point of green excitation [case (i) in Fig. 1(d)]. As the applied voltage increases, we witness a gradual distortion of the cylindrical symmetry and the formation of a dark "tail" indicative of hole drift toward the ground electrode.

To gain an understanding of the system dynamics, we first resort to a set of master equations that take into account carrier photogeneration and trapping as well as diffusive
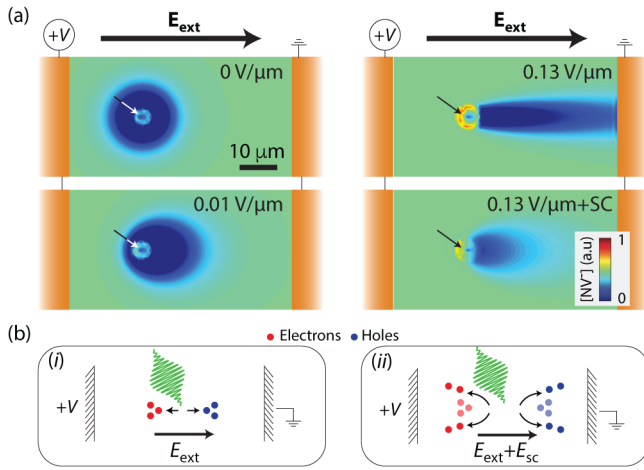
FIG. 2. Modeling space-charge potentials. (a) Numerical simulation of NV charge patterns for variable field E_{ext} assuming a diamond with NV (nitrogen) concentration of 2.5 ppb (0.25 ppm). In all calculations, the field is assumed constant throughout the sample. Arrows indicate the point of illumination assuming a beam diameter of 1 μm; the total green laser park time is 20 ms. Space-charge (SC) effects are included in the right lower plot, where the induced field is seen to reach 0.075 V/μm. (b) The application of external bias leads to charge separation and thus space-charge formation (i), subsequently altering the path of incoming carriers (ii).

FIG. 3. $\tilde{t}_E = n(t_{P1} + t_{P2})$ Charge dynamics in the presence of pulsed electric fields. (a) Experimental protocol (top left); the total parking time amounts to . [(i)–(v)] Differential NV$^-$ fluorescence maps for different applied voltages; in these experiments, $t_{P1} = 1$ ms, $t_{P2} = 1$ ms, $\tilde{t}_P = 1$ min, and the arrow denotes the direction of the externally applied electric field. (b) (Left) Same as above but for $t_{P2} = 10$ μs (right) or $t_{P2} = 0$ μs (left) at 420 V. The same color bar applies to both (a) and (b).

transport and electric-field-driven drift, using ionization and capture parameters derived previously [11]. Assuming NV charge initialization via green excitation, Fig. 2(a) shows the calculated NV charge patterns after a 100-ms-long green park for varying external fields E_{ext}. Comparison with the results in Fig. 1(d) shows the model quickly departs from our observations as it predicts the formation of distinct jetlike patterns, even at fields lower than those applied in our experiments (of order 1 V/μm). This trend changes, however, when the time-varying space-charge field created by previously trapped carriers—below referred to as the "local" contribution to the space-charge field E_{sc}—is taken into account throughout the laser park time [right lower image in Fig. 2(a); see also Supplemental Material [17]].

Although the agreement with our observations in Fig. 1 must be deemed qualitative, our modeling shows that the impact of space-charge fields on the system dynamics is amplified in the presence of externally applied potentials. Intuitively, the latter can be understood as a consequence of the charge separation taking place at early stages [Fig. 2(b)], gradually preventing carrier drift toward the electrodes and thus producing the broad, diffusivelike pattern observed experimentally. Unfortunately, using modeling alone to quantify the space-charge field in a class 1b diamond is difficult, as the type and concentration of all defects at play (including their ionization rates and trapping cross sections) is not fully known [12]. Note, however, that nitrogen impurities—presumably assuming
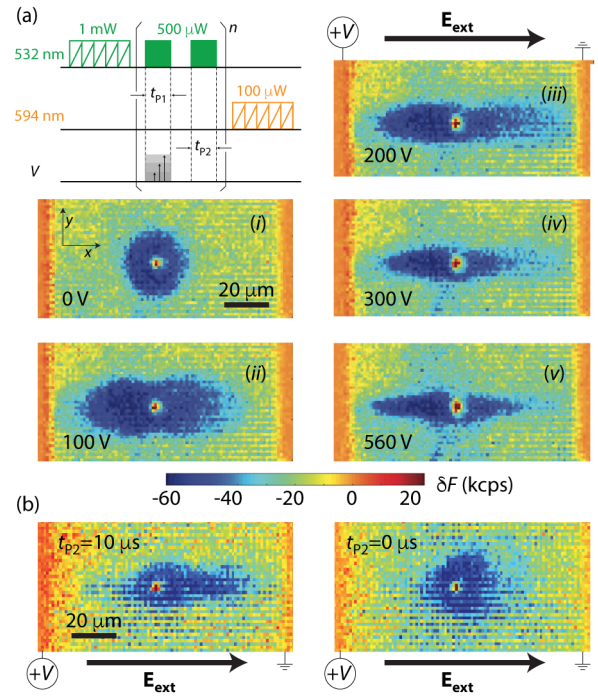
positive, neutral, and negative charge configurations via hole and (multi)electron capture [17–22]—largely outnumber NVs, implying the latter serve mainly as probes to expose the underlying dynamics.

To more directly gauge the influence of the space-charge field, we implement the experiment in Fig. 3(a). Similar to the protocol in Fig. 1(c), we charge initialize (readout) NV$^-$ via a green (orange) laser scan preceding (following) a green laser park. In this case, however, we fraction the park time into a train of n pairs of pulses, each lasting a time t_{Pj}, $j = 1, 2$, without altering the total park time $\tilde{t}_P = n(t_{P1} + t_{P2})$, which is kept identical to that in Fig. 1. Further, we use a high-speed switch to turn on (off) the electric field during t_{P1} (t_{P2}) throughout the pulse train.

Figure 3(a) shows a collection of NV$^-$ differential fluorescence images at increasing voltages. As expected, the charge pattern at zero applied voltage remains unchanged relative to the uninterrupted park [panel (i) in Fig. 1(d)] since the charge dynamics virtually freezes during the dark intervals between laser pulses [6]. As the applied voltage increases, however, the pattern evolves toward a doubly pronged, jetlike shape, dramatically different from that observed in Fig. 1 at comparable voltages. This response can be understood via the
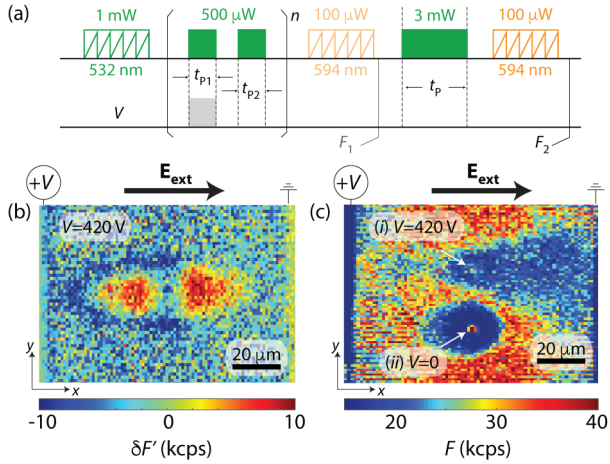
FIG 4. $\tilde{t}_P = 10$ sProbing local and nonlocal space charge. (a) Experimental protocol. F_2 denotes the final fluorescence image and F_1 is the reference image after the first orange scan (optional, shown in a faint trace). (b) Fluorescence image $\delta F' = F_2 - F_1$ upon use of the protocol in (a) for $t_{P1} = t_{P2} = 1$ ms, $n = 5000$, and . (c) Absolute NV$^-$ fluorescence image F upon consecutive, uninterrupted green laser parks at positions (i) and (ii) (arrows). The voltage is $V = 420$ V during park (i) and $V = 0$ V during park (ii); all other conditions as in Fig. 1.

conceptual framework of Fig. 2(b); namely, the space-charge field emerging after t_{P1} causes carriers created during t_{P2} to propagate in a direction opposite to that previously induced by E_{ext}, in the process neutralizing E_{sc} at the end of the nth cycle. Correspondingly, carriers produced during t_{P1} in the $(n + 1)$th cycle can propagate farther in the direction of E_{ext}, hence resulting in elongated charge patterns, each resembling those calculated in Fig. 2(a). The pattern geometry is indicative of space-charge fields comparable to those produced externally. Interestingly, we find that optimally short, voltage-free laser pulses (i.e., $0 < t_{P2} \ll t_{P1}$) are sufficient to allow the formation of narrow, one-directional propagation channels [Fig. 3(b)], suggesting that sources other than the local space-charge field—arguably neutralized during t_{P2}—must also be at play in the observations of Fig. 3(a). We return to this point later.

Much of the discussion above rests on the implicit idea that local space-charge fields combined with trap passivation can steer free carriers in particular directions, a notion we demonstrate with the experiments in Fig. 4(a). This time we create a jetlike charge pattern F_1 using green laser pulses with alternating voltage [protocol in Fig. 3(a)] and subsequently apply an uninterrupted, voltage-free green laser park to create a pattern F_2. We can then expose the impact of the preexisting charge distribution on carrier propagation through the differential NV$^-$ fluorescence image $\delta F' = F_2 - F_1$. Figure 4(b) shows the result: The dark contour on the left of the image unmistakably points to carriers propagating along the charge blueprint previously produced during the laser pulse train. Further, the fact that

the contour appears exclusively on one side of the pattern indicates that a residual, long-lasting space-charge field accelerates holes to the left. Remarkably, we also find a relative growth of NV$^-$ fluorescence within the preexisting blueprint. Unlike the dark contour, the bright pattern features two halves of comparable shape and (differential) intensity, suggesting the underlying mechanism is insensitive to the residual space-charge field. This observation could indicate the formation of excitons—whose binding energy in diamond reaches 70–80 meV [23]—though additional work will be needed to clarify the dynamics of this process.

In addition to this local contribution to the space-charge field, we find that other extended sources play an equally important role. This is shown in Fig. 4(c) where we park the green laser at two locations, (i) and (ii) for long, uninterrupted intervals (protocol in Fig. 1), differing only in the external electric field, active during the first park but not the second. Remarkably, pattern (ii) elongates in a direction opposite to pattern (i), thus revealing a nonlocal field stretching throughout the gap between the electrodes, possibly stemming from carrier traps at the metal-dielectric interface. The amplitude of the tail in pattern (ii) suggests this source of space charge is significant. Future work—for example, using the spin of near-electrode NVs as electric-field sensors [24]—could prove useful to more quantitatively determine the extent and amplitude of these fields.

In conclusion, transport of photogenerated carriers and charge trapping in adjacent defects leads to the formation of strong, metastable space-charge fields, which, in turn, play a dominant role on subsequent carrier propagation. The use of pulsed protocols articulating external voltages and carrier injection allows us to tailor the interplay between carrier propagation and space-charge field formation so as to change the carrier range and/or direction of propagation. Further, the charge patterns that emerge can serve themselves as blueprints to guide carriers along trajectories where trapping is strongly suppressed.

Several intriguing questions are in need of further exploration. For example, throughout our measurements we find that local green excitation leads to an overall reduction of NV$^-$ population far away from the point of illumination (note the slightly negative value in the background differential fluorescence of Figs. 1 and 3). While we presently cannot rule out the influence of scattered laser light, preliminary observations suggest this effect may instead derive from a form of electric-field insensitive transport, possibly via excitons or exciton complexes [25,26] formed by electron-hole binding during the laser park. Whether or not this type of process is also responsible for the "blurring" of pattern (i) in Fig. 4(c) (observed systematically across multiple analogous experiments) is a closely related question. Further examination is thus warranted, especially given the long range of this

effect—exceeding several tens of microns—suggestive of trapping-protected propagation.

As a route to probing space charge in insulators, our strategy is complementary to scanning-probe methods [9,10], higher in resolution but restricted to examining surfaces. It also provides an alternative to acoustic- or thermal-stimuli methods [27–30] in that it is light-diffraction-limited and more naturally adapted to the investigation of small defect ensembles. While the present studies focused on diamond, we anticipate comparable behavior in other wide band gap materials of technological importance. One concrete example is SiC, where charge control of SiV and double-vacancy centers has already been demonstrated and shown to produce long-lived states [31–33]. Another illustration is the family of rare-earth-doped inorganic insulators—of interest for optical information storage [34] due their long-lasting photo-chromism [35]—and lanthanide-hosting nitrides such as GaN [36]. Similar ideas could be applicable to mid- and low-band-gap semiconductors in situations where thermal activation is insufficient to establish equilibrium (e.g., systems under cryogenic conditions). Besides the fundamental aspects, our findings may prove relevant to the operation of various semiconducting devices, especially those combining regions of high and low doping (i.e., PIN junctions). Combined with photocurrent measurements, the present techniques could also find use in the investigation of solar cell operation [37,38], in studies to probe the dynamics of magnetoresistance with submicron resolution [39,40], or in the realization of novel quantum technology concepts combining charge and spin [41,42].

---

*These authors contributed equally to this work.
†Corresponding author.
cmeriles@ccny.cuny.edu

[1] N. F. Mott and R. W. Gurney, *Electronic Processes in Ionic Crystals* (Oxford University Press, London, 1940).

[2] A. Rose, Space-charge-limited currents in solids, Phys. Rev. **97**, 1538 (1955).

[3] M. A. Lampert, Simplified theory of space-charge-limited currents in an insulator with traps, Phys. Rev. **103**, 1648 (1956).

[4] H. T. Nicolai, M. M. Mandoc, and P. W. M. Blom, Electron traps in semiconducting polymers: Exponential versus Gaussian trap distribution, Phys. Rev. B **83**, 195204 (2011).

[5] X.-G. Zhang and S. T. Pantelides, Theory of Space Charge Limited Currents, Phys. Rev. Lett. **108**, 266602 (2012).

[6] S. Dhomkar, J. Henshaw, H. Jayakumar, and C. A. Meriles, Long-term data storage in diamond, Sci. Adv. **2**, e1600911 (2016).

[7] S. Dhomkar, H. Jayakumar, P. R. Zangara, and C. A. Meriles, Charge dynamics in near-surface, variable-density ensembles of nitrogen-vacancy centers in diamond, Nano Lett. **18**, 4046 (2018).

[8] M. P. Delmo, S. Yamamoto, S. Kasai, T. Ono, and K. Kobayashi, Large positive magnetoresistive effect in silicon induced by the space-charge effect, Nature (London) **457**, 1112 (2009).

[9] W. Melitz, J. Shena, A. C. Kummel, and S. Lee, Kelvin probe force microscopy and its application, Surf. Sci. Rep. **66**, 1 (2011).

[10] S. B. Kuntze, D. Ban, E. H. Sargent, S. J. Dixon-Warren, J. K. White, and K. Hinzer, Electrical scanning probe microscopy: Investigating the inner workings of electronic and optoelectronic devices, Crit. Rev. Solid State Mater. Sci. **30**, 71 (2005).

[11] S. Dhomkar, P. R. Zangara, J. Henshaw, and C. A. Meriles, On-Demand Generation of Neutral and Negatively-Charged Silicon-Vacancy Centers in Diamond, Phys. Rev. Lett. **120**, 117401 (2018).

[12] A. Lozovoi, D. Daw, H. Jayakumar, and C. A. Meriles, Dark defect charge dynamics in bulk chemical-vapor-deposition-grown diamonds probed via nitrogen vacancy centers, Phys. Rev. Mater. **4**, 053602 (2020).

[13] A. M. Edmonds, U. F. S. D'Haenens-Johansson, R. J. Cruddace, M. E. Newton, K.-M. C. Fu, C. Santori, R. G. Beausoleil, D. J. Twitchen, and M. L. Markham, Production of oriented nitrogen-vacancy color centers in synthetic diamond, Phys. Rev. B **86**, 035201 (2012).

[14] M. W. Doherty, N. B. Manson, P. Delaney, F. Jelezko, J. Wrachtrup, and L. C. L. Hollenberg, The nitrogen-vacancy colour centre in diamond, Phys. Rep. **528**, 1 (2013).

[15] N. Aslam, G. Waldherr, P. Neumann, F. Jelezko, and J. Wrachtrup, Photo-induced ionization dynamics of the nitrogen vacancy defect in diamond investigated by single-shot charge state detection, New J. Phys. **15**, 013064 (2013).

[16] H. Jayakumar, J. Henshaw, S. Dhomkar, D. Pagliero, A. Laraoui, N. B. Manson, R. Albu, M. W. Doherty, and C. A. Meriles, Optical patterning of trapped charge in nitrogen-doped diamond, Nat. Commun. **7**, 12660 (2016).

[17] See Supplemental Material at http://link.aps.org/supplemental/10.1103/PhysRevLett.125.256602 for details on modeling the diffusion and drift of photo-generated carriers.

[18] L. S. Pan, D. R. Kania, P. Pianetta, and O. L. Landen, Carrier density dependent photoconductivity in diamond, Appl. Phys. Lett. **57**, 623 (1990).

[19] S. Han in *Diamond: Electronic Properties and Applications*, edited by L. S. Pan and D. R. Kania (Springer Science, New York, 1995).

[20] J. Isberg, M. Gabrysch, J. Hammersberg, S. Majdi, K. K. Kovi, and D. J. Twitchen, Generation, transport and

detection of valley-polarized electrons in diamond, Nat. Mater. **12,** 760 (2013).

[21] R. Ulbricht, S. T. van der Post, J. P. Goss, P. R. Briddon, R. Jones, R. U. A. Khan, and M. Bonn, Single substitutional nitrogen defects revealed as electron acceptor states in diamond using ultrafast spectroscopy, Phys. Rev. B **84,** 165202 (2011).

[22] M. Nesladek, A. Bogdan, W. Deferme, N. Tranchant, and P. Bergonzo Charge transport in high mobility single crystal diamond, Diam. Relat. Mater. **17,** 1235 (2008).

[23] J. Barjon, Luminescence spectroscopy of bound excitons in diamond, Phys. Status Solidi A **214,** 1700402 (2017).

[24] F. Dolde, H. Fedder, M. W. Doherty, T. Nöbauer, F. Rempp, G. Balasubramanian, T. Wolf, F. Reinhard, L. C. L. Hollenberg, F. Jelezko, and J. Wrachtrup, Electric-field sensing using single diamond spins, Nat. Phys. **7,** 459 (2011).

[25] J. Omachi, T. Suzuki, K. Kato, N. Naka, K. Yoshioka, and M. Kuwata-Gonokami, Observation of Excitonic n-Body Bound States: P in Diamond, Phys. Rev. Lett. **111,** 026402 (2013).

[26] H. Morimoto, Y. Hazama, K. Tanaka, and N. Naka, Ultra-high exciton diffusion in intrinsic diamond, Phys. Rev. B **92,** 201202(R) (2015).

[27] S. Hole and J. Lewiner, Direct measurement of trapped and free charge distributions in semiconductors, Appl. Phys. Lett. **84,** 1308 (2004).

[28] J. L. Franceschi and V. Haas, Laser thermo-acoustic modulation for space charge measurement, Appl. Phys. Lett. **70,** 2236 (1997).

[29] A. Mellinger, R. Singh, M. Wegener, W. Wirges, R. Gerhard-Multhaupt, and S. B. Lang, Three-dimensional mapping of polarization profiles with thermal pulses, Appl. Phys. Lett. **86,** 082903 (2005).

[30] A. Cernomorcenco and P. Notingher, Jr., Application of the thermal step method to space charge measurements in inhomogeneous solid insulating structures: A theoretical approach, Appl. Phys. Lett. **93,** 192903 (2008).

[31] G. Wolfowicz, C. P. Anderson, A. L. Yeats, S. J. Whiteley, J. Niklas, O. G. Poluektov, F. J. Heremans, and D. D. Awschalom, Optical charge state control of spin defects in 4H-SiC, Nat. Commun. **8,** 1876 (2017).

[32] D. A. Golter and C. W. Lai, Optical switching of defect charge states in 4H-SiC, Sci. Rep. **7,** 13406 (2017).

[33] M. Widmann, M. Niethammer, D. Y. Fedyanin, I. A. Khramtsov, T. Rendler, I. D. Booker, J. U. Hassan, N. Morioka, Y.-C. Chen, I. G. Ivanov, N. T. Son, T. Ohshima, M. Bockstedte, A. Gali, C. Bonato, S.-Y. Lee, and J. Wrachtrup, Electrical charge state manipulation of single silicon vacancies in a silicon carbide quantum opto-electronic device, Nano Lett. **19,** 7173 (2019).

[34] D. Liu, L. Yuan, Y. Jin, H. Wu, Y. Lv, G. Xiong, G. Ju, L. Chen, S. Yang, and Y. Hu, Tailoring multidimensional traps for rewritable multilevel optical data storage, ACS Appl. Mater. Interfaces **11,** 35023 (2019).

[35] N. Riesen, X. Pan, K. Badek, Y. Ruan, T. M. Monro, J. Zhao, H. Ebendorff-Heidepriem, and H. Riesen, Towards rewritable multilevel optical data storage in single nano-crystals, Opt. Express **26,** 12266 (2018).

[36] B. Mitchell, N. Hernandez, D. Lee, A. Koizumi, Y. Fujiwara, and V. Dierolf, Charge state of vacancy defects in Eu-doped GaN, Phys. Rev. B **96,** 064308 (2017).

[37] F. Deledalle, T. Kirchartz, M. S. Vezie, M. Campoy-Quiles, P. S. Tuladhar, J. Nelson, and J. R. Durrant, Understanding the Effect of Unintentional Doping on Transport Optimization and Analysis in Efficient Organic Bulk-Heterojunction Solar Cells, Phys. Rev. X **5,** 011032 (2015).

[38] O. J. Sandberg, S. Dahlström, M. Nyman, S. Wilken, D. Scheunemann, and R. Österback, Impact of a Doping-Induced Space-Charge Region on the Collection of Photo-generated Charge Carriers in Thin-Film Solar Cells Based on Low-Mobility Semiconductors, Phys. Rev. Applied **12,** 034008 (2019).

[39] M. P. Delmo, S. Yamamoto, S. Kasai, T. Ono, and K. Kobayashi, Large positive magnetoresistive effect in silicon induced by the space-charge effect, Nature (London) **457,** 1112 (2009).

[40] Y. Liu, H. Wang, X. Jin, and M. Zhang, The space charge limited current and huge linear magnetoresistance in silicon, Sci. Rep. **8,** 775 (2018).

[41] P. Siyushev, M. Nesladek, E. Bourgeois, M. Gulka, J. Hruby, T. Yamamoto, M. Trupke, T. Teraji, J. Isoya, and F. Jelezko, Photoelectrical imaging and coherent spin-state readout of single nitrogen-vacancy centers in diamond, Science **363,** 728 (2019).

[42] M. W. Doherty, C. A. Meriles, A. Alkauskas, H. Fedder, M. J. Sellars, and N. B. Manson, Towards a Room-Temperature Spin Quantum Bus in Diamond via Optical Spin Injection, Transport and Detection, Phys. Rev. X **6,** 041035 (2016).